



# Numerical Modeling of Stability of Fractured Reservoir Bank Slopes Subjected to Water–Rock Interactions

Zhihong Zhao<sup>1</sup> · Tiecheng Guo<sup>1</sup> · Zeyu Ning<sup>3</sup> · Zihao Dou<sup>1</sup> · Feng Dai<sup>2</sup> · Qiang Yang<sup>3</sup>

Received: 15 April 2017 / Accepted: 5 November 2017 / Published online: 16 November 2017  
© Springer-Verlag GmbH Austria, part of Springer Nature 2017

## Abstract

The effect of water on the shear behavior of joints in rocks is critical for determining the global stability of fractured rock slopes subjected to changes in water levels, because the joint peak shear strength can be significantly lowered owing to wetting. The roles of the mechanical and the combined physical and chemical water–rock interactions in the deformation of reservoir bank slopes are studied using discrete element method. The numerical results showed that the joints that are subparallel to the slope surface mainly determine the displacements of rock blocks and that water–rock interaction-induced deterioration of joint shear stiffness and strength plays a critical role in the stability of reservoir bank slopes. The weakening of rock fractures induced by interactions between water and fracture walls can explain the monitored valley contraction during the impoundment of high dams.

**Keywords** Rock fracture · Reservoir bank slopes · Water–rock interactions · Discrete element model · Valley contraction

## List of symbols

$E$	Young's modulus (GPa)	$\Delta u_n$	Normal displacement increment (m)
$\nu$	Poisson's ratio	$\sigma'_n$	Effective normal stress (Pa)
$a$	Fracture hydraulic aperture (m)	$\Delta\sigma'_n$	Effective normal stress increment (Pa)
$a_o$	Fracture hydraulic aperture at zero normal stress (m)	$\Delta\tau_s$	Shear stress increment (Pa)
$a_{res}$	Minimum (or residual) aperture value (m)	$\Delta u_s^e$	Elastic component of incremental shear displacement (m)
$k_j$	Fracture permeability factor ( $\text{Pa}^{-1} \text{s}^{-1}$ )	$\tau$	Fracture shear strength (Pa)
$k_n$	Fracture normal stiffness ( $\text{Pa m}^{-1}$ )	$c$	Fracture cohesion strength (Pa)
$k_s$	Fracture shear stiffness ( $\text{Pa m}^{-1}$ )	$\varphi$	Fracture friction angle ( $^\circ$ )
$l$	Fracture length (m)	$\mu$	Dynamic viscosity of the fluid (Pa s)
$p$	Water pressure (Pa)		
$\Delta p$	Fluid pressure difference (Pa)		
$q$	Fluid flow rate ( $\text{m}^2 \text{s}^{-1}$ )		
$u_n$	Normal displacement (m)		

✉ Zhihong Zhao  
zhzhao@tsinghua.edu.cn

✉ Feng Dai  
fengdai@scu.edu.cn

<sup>1</sup> Department of Civil Engineering, Tsinghua University, Beijing, China

<sup>2</sup> State Key Laboratory of Hydraulics and Mountain River Engineering, College of Water Resources and Hydropower, Sichuan University, Chengdu, China

<sup>3</sup> State Key Laboratory of Hydroscience and Engineering, Tsinghua University, Beijing, China

## 1 Introduction

Water is one of the most important environmental factors controlling the stability of fractured rock slopes. Impoundment of reservoirs can induce various magnitudes of bank slope deformation or even landslides. The heavily fractured left-abutment slope of the Beaugard dam on the Dora di Valgrisenche River of northwestern Italy has experienced significant displacements since the early days of reservoir filling in the 1960s (Barla et al. 2010). Obviously, accelerated valley contractions and slope displacements were monitored during the initial impoundment of the Lijiaxia, Jinping I and Xiluodu dams in China (Cheng et al. 2017). However, the relationship between reservoir water levels and displacements of reservoir slopes still remains poorly

understood, and studying the deformation mechanisms of fractured reservoir slopes during impoundment is fundamental to dam safety.

Conventionally, the effects of water are only considered as either mechanical loads applied on the slope surfaces, assuming that rock masses are impermeable, or as a seepage force, based on Terzaghi's effective stress principle and Biot's effective stress coefficient (Maihemuti et al. 2016). Bidgoli and Jing (2015) performed discrete element modeling of the coupled stress–deformation–flow processes in a fractured rock mass and found that water pressure has a significant influence on the macroscopic strength of fractured rock masses, but a minor effect on their elastic deformation parameters.

It has been observed that various types of rocks could suffer a significant loss of compressive and tensile strengths upon saturation (Wasantha and Ranjith 2014; Cherblanc et al. 2016; Zhao et al. 2017a; Qiao et al. 2017). The four main mechanisms of interactions between water and rocks are as follows (Van Eeckhout 1976): (1) fracture energy reduction, (2) capillary tension decrease, (3) frictional reduction and (4) chemical and corrosive deterioration. Ciantia et al. (2015a, b) identified two distinct types of bonding within calcarenites: temporary bonding (TB) and persistent bonding (PB), which are responsible for the observed rapid decrease in rock strength when water fills the pores (a short-term effect), and a long-term weakening of saturated rocks (a long-term effect).

In addition, Pellet et al. (2013) showed that the shear strength of marl fractures is strongly dependent on water content, i.e., the friction angle drops from 22° for a dry fracture to 12° for a saturated fracture, and the fracture cohesion decreases from 0.41 MPa under dry conditions to 0.32 MPa under wet conditions. Chen et al. (2014) found that the average asperity height of various rock fractures increased after immersion in an in situ solution of pH 7.1 for 30 days. Recent experimental studies by the authors showed that the peak shear strength of sawtooth sandstone fractures can be lowered by about 20–24% due to wetting (Zhao et al. 2017b), but the saturation-induced reduction in joint shear strength is probably not sensitive to the duration of immersion. Note that the tested sandstone was a fine-grained feldspathic arenite containing ≤ 2% clayey matrix and sparse calcite cement. However, this mechanism of wetting-induced strength reductions in rocks and fractures was commonly neglected in previous stability analyses of fractured reservoir slopes.

The main objective of this study is to clarify the effects of water pressures and wetting-induced weakening of fractures on stability of fractured reservoir slopes. Two numerical benchmark examples were solved to evaluate the contributions of water pressures and wetting-induced weakening of fractures to fractured slope displacements. Finally, a case

study of the right reservoir bank slopes of the Jinping I dam is presented.

## 2 Review of Effects of Water–Rock Interactions on Fracture Behavior

The introduction of water into rock fractures may modify the mechanical properties of fractured rock masses in two main ways: (1) a purely mechanical effect of pore pressure, i.e., the classical effective stress principle, and (2) physicochemical interactions between water and fracture walls, including lubrication, softening, argillation and scouring (Jaeger et al. 2007).

### 2.1 Mechanical Effects of Water–Rock Interactions

When water pressure is present in fracture voids, the fracture surfaces are forced apart and the normal stress,  $\sigma_n$ , is reduced. Under a steady-state condition, where there is sufficient time for the water pressures in fractures to reach equilibrium, the reduced normal stress,  $\sigma'_n$ , is defined as,

$$\sigma'_n = \sigma_n - p \quad (1)$$

where  $p$  is the water pressure. The reduced normal stress  $\sigma'_n$  is usually called the effective normal stress. The mechanical effect of water pressure on deformation, strength and hydraulic aperture of fractures can be calculated through the constitutive laws or strength criterion of fractures (Jing and Stephansson 2007). Tuncay and Corapcioglu (1995) derived an effective stress principle for saturated fractured porous rocks based on the double-porosity representation. In this study, we assumed that intact rocks were impermeable, and thus, Eq. (1) was used to calculate the effective normal stress applied on fracture walls.

### 2.2 Physicochemical Effects of Water–Rock Interactions

A number of experimental studies have shown that under the combination of the physicochemical interactions between water and fracture walls, joint wall compressive strengths and basic friction angles can be reduced by about 5–20 and 0–45%, respectively, upon saturation (Barton and Choubey 1977; Geertsema 2003; Pellet et al. 2013). In addition, we found that the average peak shear strength of irregular granite fractures changed from 10.2 MPa when dry to 8.5 MPa after immersion in water for 90 days, a reduction of about 17%. Using a hypothetical example of a steep rock slope, Zhao et al. (2017b) showed that only considering the purely mechanical effect of pore pressure, but neglecting the wetting-induced weakening of rock joints, may overestimate slope stability and be highly risky for practical rock

engineering. In this study, we further attempt to examine the role of physicochemical water–rock interaction-induced reductions in fracture shear stiffnesses and strengths in reservoir slope deformation.

### 3 Numerical Studies

#### 3.1 Discrete Element Method

The two-dimensional universal distinct element code (UDEC) was adopted in this study (Itasca Consulting Group Inc 2014). Intact rocks were approximated as linear, isotropic, homogeneous and elastic materials. Deformation of the rock matrix was described simply by two elastic constants, Young’s modulus ( $E$ ) and Poisson’s ratio ( $\nu$ ). Intact rocks were assumed to be impermeable, and water only flowed through connected fractures. We considered the fully coupled mechanical–hydraulic processes in fractures, in which fracture conductivity was dependent on mechanical deformation and, conversely, fracture fluid pressures affected the mechanical computations.

The Coulomb slip model in UDEC was used to represent the mechanical behavior of rock fractures. In the normal direction, the stress–displacement relation is assumed to be linear and governed by fracture normal stiffness,  $k_n$ ,

$$\Delta\sigma'_n = -k_n\Delta u_n \tag{2}$$

where  $\Delta\sigma'_n$  is effective normal stress increment and  $\Delta u_n$  is the normal displacement increment. In the shear direction, shear stress–displacement is similarly governed by fracture shear stiffness,  $k_s$ ,

$$\Delta\tau_s = -k_s\Delta u_s^e \tag{3}$$

where  $\Delta\tau_s$  is the shear stress increment and  $\Delta u_s^e$  is the elastic component of incremental shear displacement.

The fracture shear strength is described by the Mohr–Coulomb criterion,

$$\tau = \sigma'_n \tan \varphi + c \tag{4}$$

where  $\tau$  is fracture shear strength;  $\varphi$  is fracture friction angle; and  $c$  is fracture cohesion.

The water flow rate in rock fractures is governed by the cubic law,

$$q = -k_j a^3 \frac{\Delta p}{l} \tag{5}$$

where  $q$  is the fluid flow rate;  $k_j = 1/12\mu$  is a fracture permeability factor;  $a$  is the fracture hydraulic aperture;  $l$  is the fracture length; and  $\Delta p$  is the fluid pressure difference.

Generally, the hydraulic aperture is given by Eq. (6),

$$a = a_o + u_n \tag{6}$$

where  $a_o$  is the joint aperture at zero normal stress and  $u_n$  is the normal displacement increment. A minimum aperture value  $a_{res}$  is assumed, below which hydraulic aperture is not affected by joint normal displacement.

#### 3.2 Model Setup

Two idealized reservoir bank slopes were designed to investigate the effect of water–rock interactions on the stability of fractured rock slopes. The models were 350 m in width and 150 m in height. The reservoir depth was 100 m, and the bank slope angle was 80°. In the idealized reservoir bank slope I, there was one set of joints tilting at  $-45^\circ$ , spaced at 20 m apart (Fig. 1a). In idealized reservoir bank slope II, three sets of joints existed in the slope, and their inclination angles and spacings were  $-45^\circ$ ,  $30^\circ$  and  $60^\circ$ ; and 40, 30 and 20 m, respectively (Fig. 1b). The parameters of rock blocks and fractures are given in Table 1. Fracture normal stiffness  $k_n$  was derived from fracture shear stiffness  $k_s$  according to the empirical relation  $k_n/k_s = 10$ , which can be used for shallow fractured rocks (Rode et al. 1991). Wetting-induced weakening of intact rocks was not considered in this study. The fluid properties in the joints are also listed in Table 1. As the final steady-state condition was of interest, the steady-state flow algorithm was adopted in the simulation, in which the influence of the fluid stiffness was eliminated. The compressibility effect of water is unimportant for steady-state flow (Zimmerman and Bodvarsson 1996).

Both of the idealized reservoir bank slopes were assigned the same mechanical and hydraulic boundary conditions. The side and bottom boundaries of the numerical models were fixed with rollers. The bottom boundary was set to be impermeable. Sufficient calculation steps were performed to reach an initial equilibrium state under gravity. Before reservoir impoundment, the water level was the bottom of the reservoir (elevation of 0 m). After impoundment, water level rose from the elevation of 0 m to 100 m, while the water level was assumed to be unchanged on the right boundary. The weight of the reservoir water was simulated by applying the equivalent pressure of 100 m of water head to the reservoir bottom and a linear changing pressure on the slope surface (Fig. 1).

#### 3.3 Modeling Procedure

Two scenarios were considered to examine the roles of the purely mechanical effect of pore pressure and the weakening of physicochemical interactions between water and fracture walls. In scenario I, only the purely mechanical effect of pore pressure was considered according to the principle of effective stress (Eq. 1). Water pressure affects normal displacements of fractures and reduces fracture shear strength by reducing effective normal stress, whereas the frictional

**Fig. 1** Geometry of idealized reservoir bank slopes. **a** Idealized reservoir bank slope I. **b** Idealized reservoir bank slope II

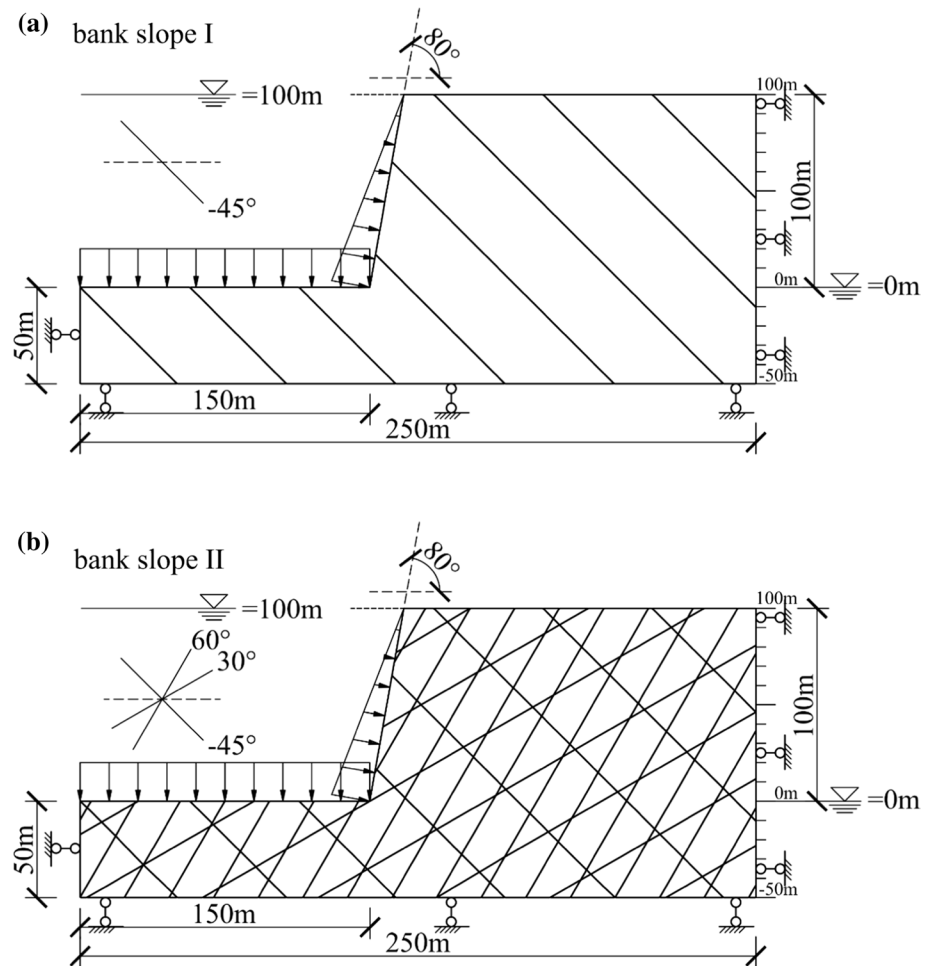


**Table 1** Mechanics properties of intact rocks and joints

Parameters (units)		Values	
		Dry	Wet
Fractured rocks	Rock density ( $\text{kg m}^{-3}$ )	2750	
	Rock Young's modulus (GPa)	10	
	Rock Poisson's ratio ( $\nu$ )	0.25	
	Fracture normal stiffness ( $\text{GPa m}^{-1}$ )	330	70 or 165
	Fracture shear stiffness ( $\text{GPa m}^{-1}$ )	33	7 or 16.5
	Fracture friction angle ( $^\circ$ )	53	46
	Fracture cohesion strength (MPa)	0.2	0.1
Fluid	Density ( $\text{kg m}^{-3}$ )	1000	
	Fracture permeability factor ( $\text{MPa}^{-1} \text{s}^{-1}$ )	$10^8$	
	Fracture aperture at zero normal stress (mm)	0.5	
	Residual joint aperture (mm)	0.2	

strength parameters ( $c$  and  $\varphi$ ) do not reduce for fractures that were immersed in water. In scenario II, the deterioration of fracture strength and fracture stiffness owing to physico-chemical water–rock interactions was considered, to clarify the effect of wetting-induced deterioration on the stability of fractured slopes. Based on the previous experimental results

(Barton and Choubey 1977; Geertsema 2003; Pellet et al. 2013; Zhao et al. 2017b), the fractures immersed in water due to impoundment were assumed to have significant shear strength deterioration. This was considered by reducing the fracture friction angle and cohesion in the present simulation (Table 1). There would be an approximate reduction in

shear strength of 25% under the effective normal stress of 1 MPa. Under other stress levels, the fracture shear stiffness was lowered by 80%, according to the laboratory experiment (Zhao et al. 2017b).

### 3.4 Results

The flow rate distributions, displacement vector fields and fracture shear displacements of the idealized reservoir bank slopes after impoundment are shown in Figs. 2, 3, 4.

#### 3.4.1 Effect of Fracture Geometry

The main difference between the two idealized reservoir bank slopes is the joint distribution. Only one set of joints dipping at  $-45^\circ$  and spaced at 40 m apart existed in the idealized reservoir bank slope I, while three sets of joints existed in the idealized reservoir bank slope II, in which two of them dip in the similar direction parallel with the bank slope surface. As a result of sparse fractures and the impermeable bottom boundary, fluid flow did not occur in the idealized reservoir bank slope I. Therefore, the effect of water was considered as mechanical loads applied on the slope surfaces.

As the water level rose from an elevation of 0 m to 100 m, the displacement vectors at the bottom of the reservoir

mainly pointed downward, and the displacement vectors along the slope surfaces mainly pointed inward (Fig. 3a). The term *inward* is used to indicate the directions of horizontal displacements toward the center of the reservoir, which represents valley contraction. The term *outward* indicates the opposite direction of horizontal displacement toward the slope and away from the center of the reservoir. The maximum displacement was 6.77 mm near to the toe of the slope. This pattern of rock displacements was beneficial to reservoir bank slope safety. In scenario I of the idealized reservoir bank slope II, water flows mainly through the fractures with inclination angle of  $-45^\circ$  and  $30^\circ$ , from the reservoir to the right boundary (Fig. 2a). In the idealized reservoir bank slope II, as the water level rose, the displacement vectors at the bottom of the reservoir mainly pointed downward, as they did for idealized reservoir bank slope I. Along the surface of idealized reservoir bank slope II, the displacement vectors pointed outward, but vertical displacement increased as height increased. It is worth noting that the displacement vectors pointed inward at the top of the slope, where a maximum rock displacement of 13.3 mm occurred. Although the trend of bedding slip appeared in the rock blocks, the slope was in a safe state.

The different rock displacement patterns between the two idealized reservoir bank slopes were mainly caused by the joints that dipped at  $60^\circ$ . Figure 4 shows the fracture shear

**Fig. 2** Flow rate distributions in idealized reservoir bank slope II. **a** Scenario I. **b** Scenario II

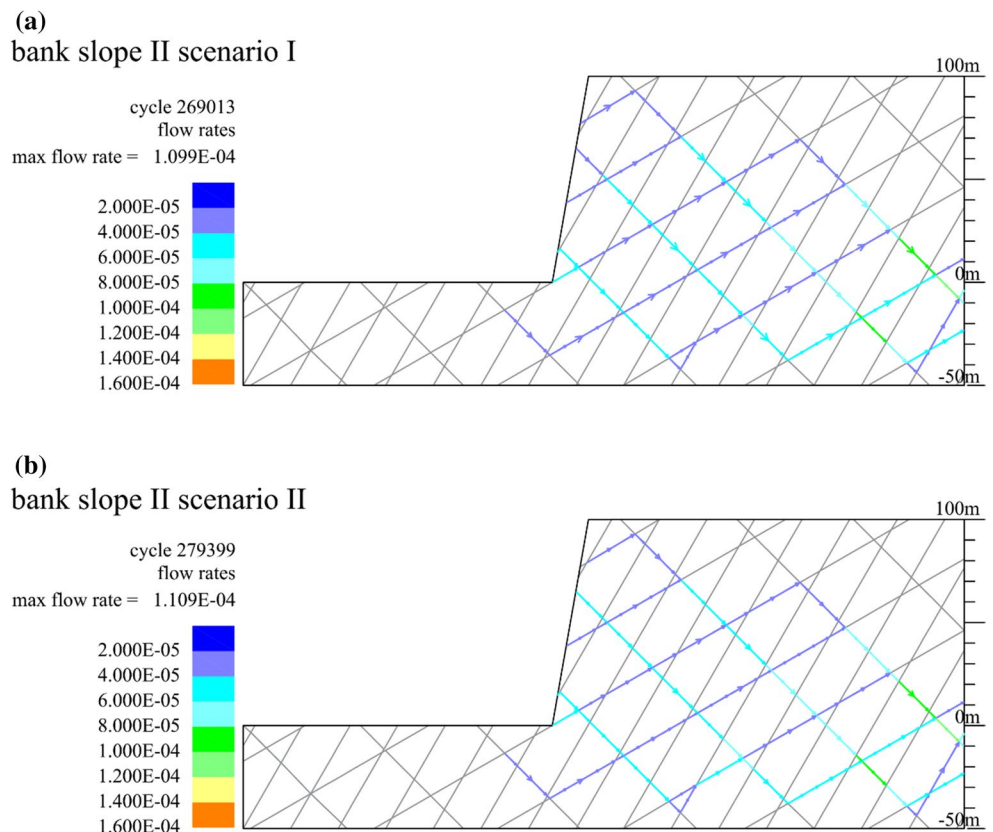
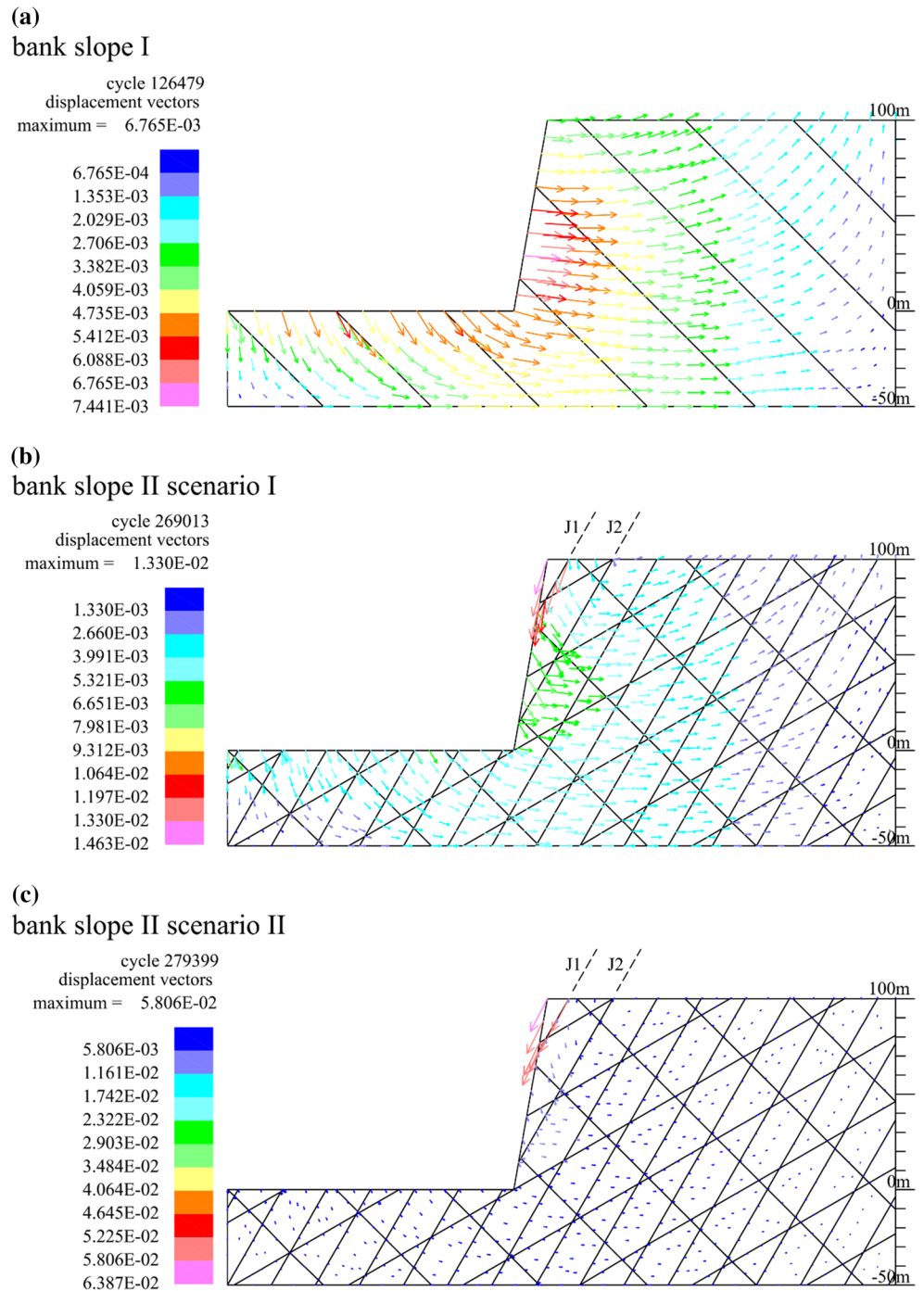


**Fig. 3** Displacement field of idealized reservoir bank slopes. **a** Idealized reservoir bank slope I. **b** Scenario I for Idealized reservoir bank slope II. **c** Scenario II for Idealized reservoir bank slope II

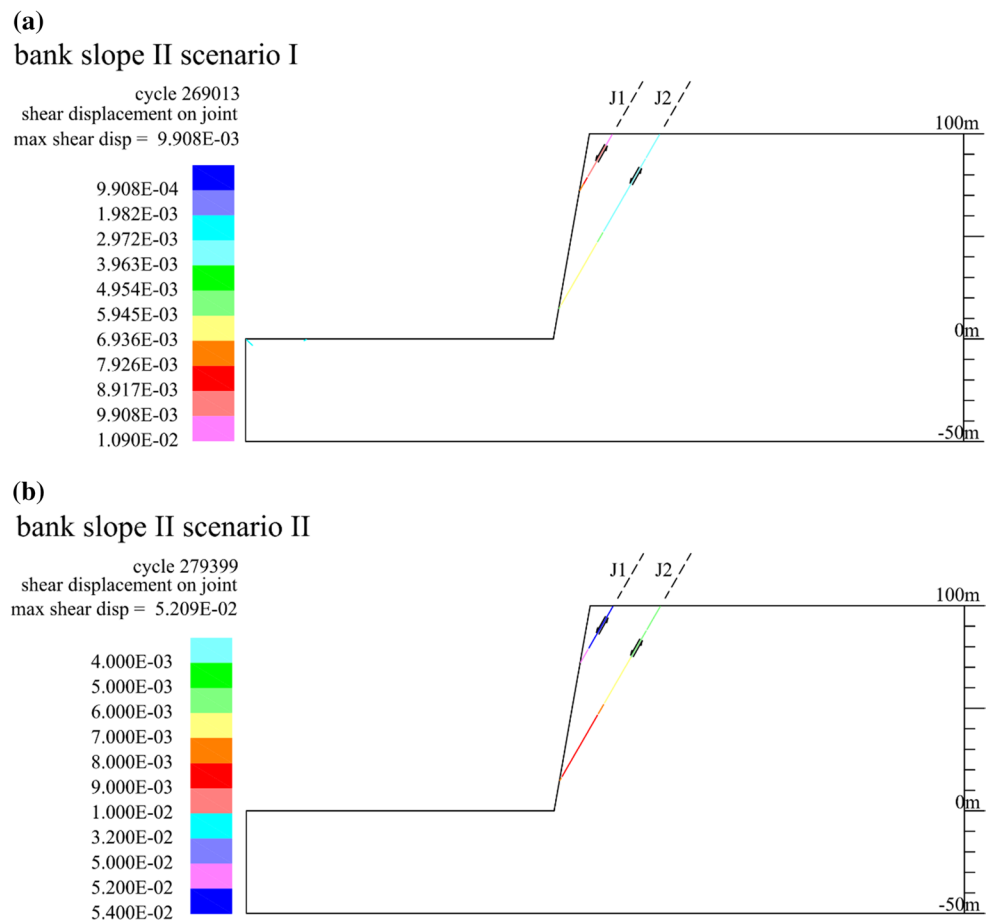


displacement of idealized reservoir bank slope II. There were large shear displacements in joints J1 and J2, for which dip angles were both  $60^\circ$ . The large joint shear displacement caused the upper half of the slope to slip outwards along the rock joints. The maximum fracture shear displacement was 9.9 mm for idealized reservoir bank slope II.

### 3.4.2 Effect of Water–Rock Interactions

To investigate the influence of physicochemical effects of water–rock interactions on the stability of reservoir bank slopes, shear strengths and joint shear stiffnesses of rock joints that were immersed in water after reservoir impoundment were reduced. In scenario II, there was similar flow rate distribution to that in scenario I, including both flow

**Fig. 4** Shear displacements in idealized reservoir bank slope II. **a** Scenario I. **b** Scenario II



path and flow rate magnitude (Fig. 2b). Water flowed mainly through the fractures with inclination angles of  $-45^\circ$  and  $30^\circ$ , from the reservoir to the right boundary. Figure 3c shows the displacement vectors in scenario II for idealized reservoir bank slope II. The displacement vectors at the bottom of the reservoir mainly pointed downward, and the displacement vectors at the slope top mainly pointed inward. The maximum rock displacement was 58.1 mm at the top of the bank slope, which was much greater than that in scenario I. This means that slope failure might be in a failure state, which was mainly caused by the failure of joint J1 that dipped at  $60^\circ$ , i.e., shear displacement of 52.1 mm (Fig. 4b). Fracture shear strength and shear stiffness were reduced due to water filling, and thus, shear stress in the fracture reached the shear strength.

#### 4 Case Study of Reservoir Bank Slope at Jinping I High Arch Dam

During the reservoir impoundment at Jinping I hydropower station, China, a significant valley contraction was monitored, which drew great concern from engineers and researchers. Cheng et al. (2017) posited that the slope

deformation during impoundment was the plastic deformation induced by the effective stress. In this case study, the possible role of water–rock interactions in valley contraction is discussed. Three numerical scenarios were separately considered based on the engineering geological conditions of Jinping I high arch dam. In the first scenario, only the purely mechanical effect of pore pressure was considered. In the second scenario, the physicochemical effects of water–rock interactions were added, to examine the relationships between reservoir water level and displacements of the bank slope. In addition, scenario III examining the sensitivity of joint stiffness reduction was also considered, to examine the effects of different reduction magnitudes of joint stiffness on displacements of the bank slope.

##### 4.1 Engineering Geological Conditions

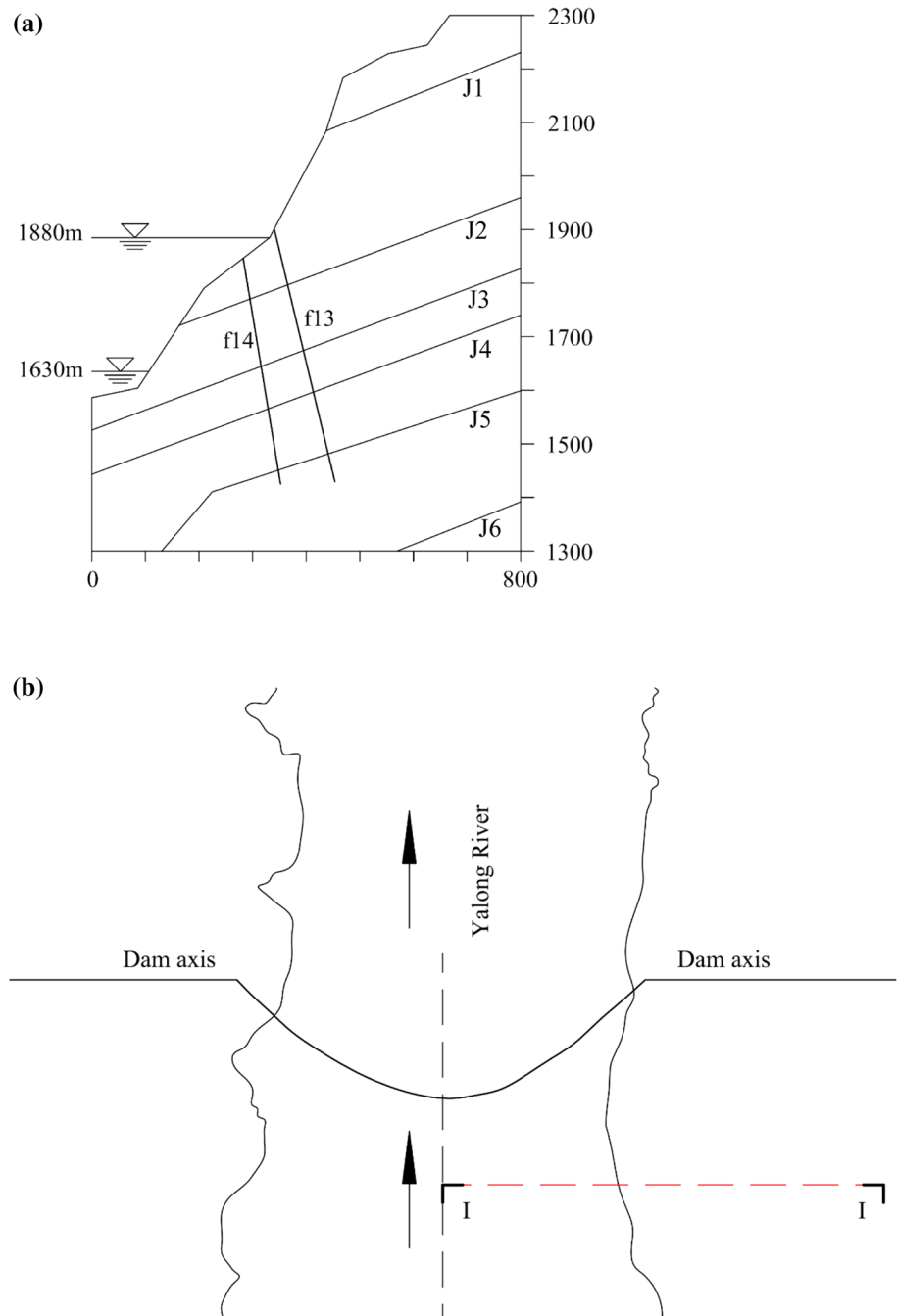
Jinping I high arch dam is located on the Yalongjiang River, China, as a controlling cascade hydropower station in the middle and downstream of the main stem, with a 305-m-high double-curvature arch dam, which is the highest arch dam in China. The total reservoir capacity is  $7.76 \times 10^9 \text{ m}^3$  at a reservoir water level of 1880 m above sea level. At the dam site, the Yalongjiang River flows in the direction  $N25^\circ E$ , with a

natural reservoir water level of 1630 m above sea level in the dry season (Qi et al. 2004). Figure 5 shows the studied section I–I of the reservoir bank slope, which is located upstream of the Jinping I high arch dam on the right side of the valley. Complex geological structures and variable strata, together with the 250-m-high water impoundment, can affect the stability of the bank slope. Strata dip to the opposite direction of the bank slope. Weak discontinuities, mainly in the presence of faults and interlayers, are developed in rock masses. Some large-scale weak discontinuities are faults f13 and f14 in the right bank (Song et al. 2013).

## 4.2 Model Setup

The numerical model is 800 m in width and 1000 m in height (Fig. 5a). In the simulation of the right bank slope at Jinping I high arch dam, rock blocks were treated as impermeable materials. Owing to the lack of the accurate in situ test data, the rock masses and fractures were assumed to be the same as those in Table 1. Fluid properties are also given in Table 1. Roller boundaries were assigned on the left, right and bottom boundaries of the model. Sufficient calculation steps were cycled before impoundment to decrease

**Fig. 5** Geometry of the right bank slope at Jinping I high arch dam. **a** Geological section I–I of right bank slope at Jinping I high arch dam. **b** Location of the modeled section across the reservoir





the unbalanced force induced under gravity. The bottom boundary was set to be impermeable. After impoundment, the water level rose by 250 m, i.e., from the elevation of 1630–1880 m in the reservoir (Fig. 5). Meanwhile, water level rose from the elevation of 1630–1780 m on the right boundary. To consider the physicochemical effects of water–rock interactions in scenario II, fracture shear strength deterioration was considered by reducing the friction angle and cohesion (Table 1). In scenario III, deteriorations of joint strength and rock stiffness were similarly considered, except the reduction magnitudes of joint stiffness. Joint normal stiffness and joint shear stiffness were 50% of those under dry condition, compared with 20% in scenario II, i.e., the joint shear stiffness was  $16.5 \text{ GPa m}^{-1}$  and the joint normal stiffness was  $165 \text{ GPa m}^{-1}$  under wet conditions in scenario III.

### 4.3 Results

Water pressure distribution in the right bank slope is plotted in Fig. 6; water pressure less than 0.5 MPa was not plotted. Fracture water pressure distributions had no obvious differences between the three numerical scenarios. Therefore, water flowed mainly through the faults f13 and f14 and the fractures between rock strata, from the reservoir to the right boundary in the three numerical scenarios (Fig. 7).

#### 4.3.1 Scenario I

The displacement field of the right bank slope in scenario I is shown in Fig. 8a. Below the water level, the main direction of rock displacements was downward at the bottom of the reservoir, and the subsidence was 44.35 mm after reservoir impoundment. Along the slope surface, the displacement vectors near the valley bottom mainly pointed outward, whereas displacement vectors pointed inward above the fracture J2. The displacement vectors pointed outward further inside of the slope below the fracture J2. The change of displacement direction was mainly caused by a large shear displacement in the fracture J2 that dipped at  $21^\circ$  (Fig. 9a). Therefore, the fracture J2 is the key fracture controlling the stability of the rock block divided by the fracture and fault f14.

The maximum fracture shear displacement was 65.76 mm, resulting in the bank above the fracture slipping down along the fracture (Fig. 9a). In the simulation, valley contraction was monitored above the river water level. The horizontal distance between the right bank and the middle line of the valley decreased by 3.33 mm at the elevation of 1980 m (100 m above the normal pool level) and decreased by 2.75 mm at the elevation of 2080 m (200 m above the normal pool level).

#### 4.3.2 Scenario II

The rock displacement field was similar to that of scenario I (Fig. 8b). Below the water level, the main direction of rock displacement pointed downward at the bottom of the river, and rock subsidence is 42.91 mm under reservoir impoundment. Along the slope surface, the displacement vectors near the valley bottom mainly pointed outward, whereas displacement vectors pointed inward above the fracture J2. The displacement vectors pointed outward further inside of the slope below the fracture J2. Fracture shear displacement showed a significant increase in the fracture J2 (Fig. 9b). The maximum fracture shear displacement was 65.76 mm, which increased by 20.1% compared with scenario I. This increase caused the slip displacement in the bank slope above this fracture to be further aggravated.

The valley width decreased by 4.97 mm at the elevation of 100 m above the pool level and decreased by 3.87 mm at the elevation of 200 m above the pool level. The valley contraction was increased by more than 40% compared with scenario I. According to in situ monitoring (Yang et al. 2015), the decrease in valley width was approximately 10 mm in the water storage period of Jingping I high arch dam. This study only considered the right bank slope, and the numerical simulation was about half of the monitored value of global valley contraction. Therefore, the magnitude of valley contraction from this numerical modeling was comparable with the monitored data at Jinping I high arc dam site, and this means that considering the mechanical and physicochemical interactions between water and fractures could explain the reason for the valley contraction.

#### 4.3.3 Scenario III

The rock displacement field of the right bank slope in scenario III is shown in Fig. 8c, and rock deformation was similar to that in scenarios I and II. The rock subsidence was 43.46 mm under reservoir impoundment at the bottom of the valley, which was almost the same as in scenario II. Along the slope surface, the displacement vectors near the valley bottom mainly pointed outward, whereas displacement vectors pointed inward above the fracture J2. The displacement vectors pointed outward further inside of the slope below the fracture J2. The maximum shear displacement value was between scenarios I and II (Fig. 9c).

The valley width decreased by 4.30 mm at the elevation of 100 m above the pool level and decreased by 3.42 mm at the elevation of 200 m above the pool level. The valley contraction values were between those in scenarios I and II as the joint stiffness values were between those of scenarios I and II. Valley contraction increases as the wet joint stiffness decreases. This indicates that the physicochemical effect of

**Fig. 6** Water pressure distribution in right bank slope of Jinping I high arch dam. **a** Scenario I. **b** Scenario II. **c** Scenario III

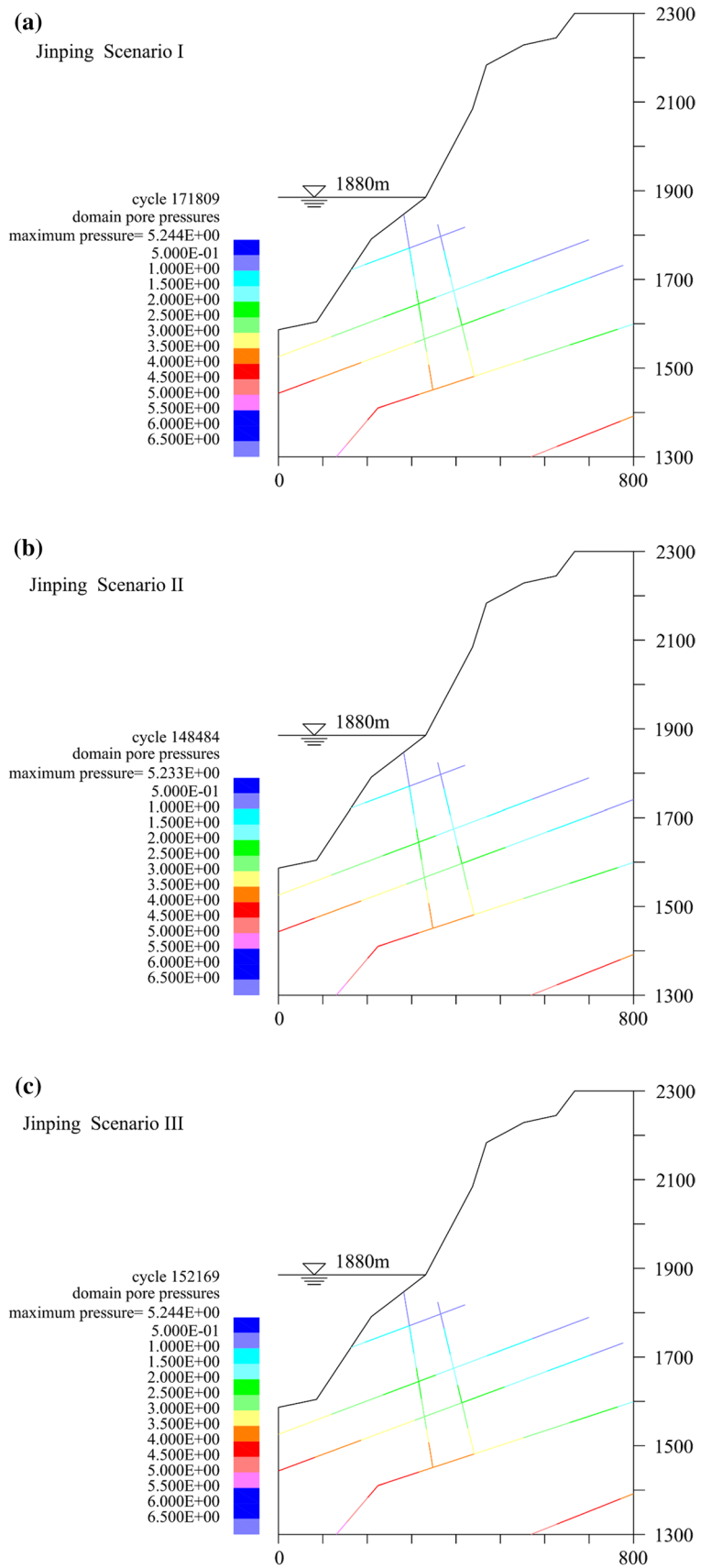


**Fig. 7** Flow rate distributions in right bank slope of Jinping I high arch dam. **a** Scenario I. **b** Scenario II. **c** Scenario III

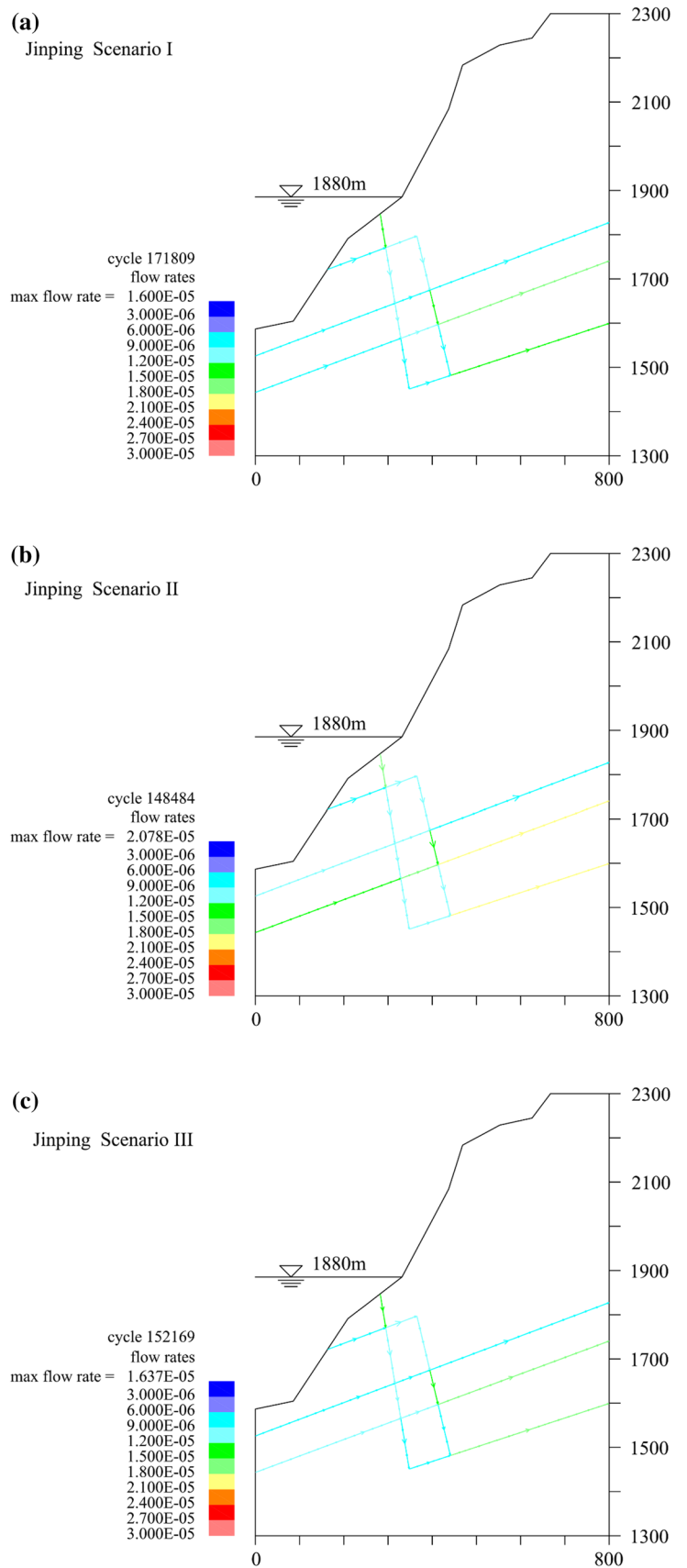


**Fig. 8** Displacement field of right bank slope of Jinping I high arch dam. **a** Scenario I. **b** Scenario II. **c** Scenario III

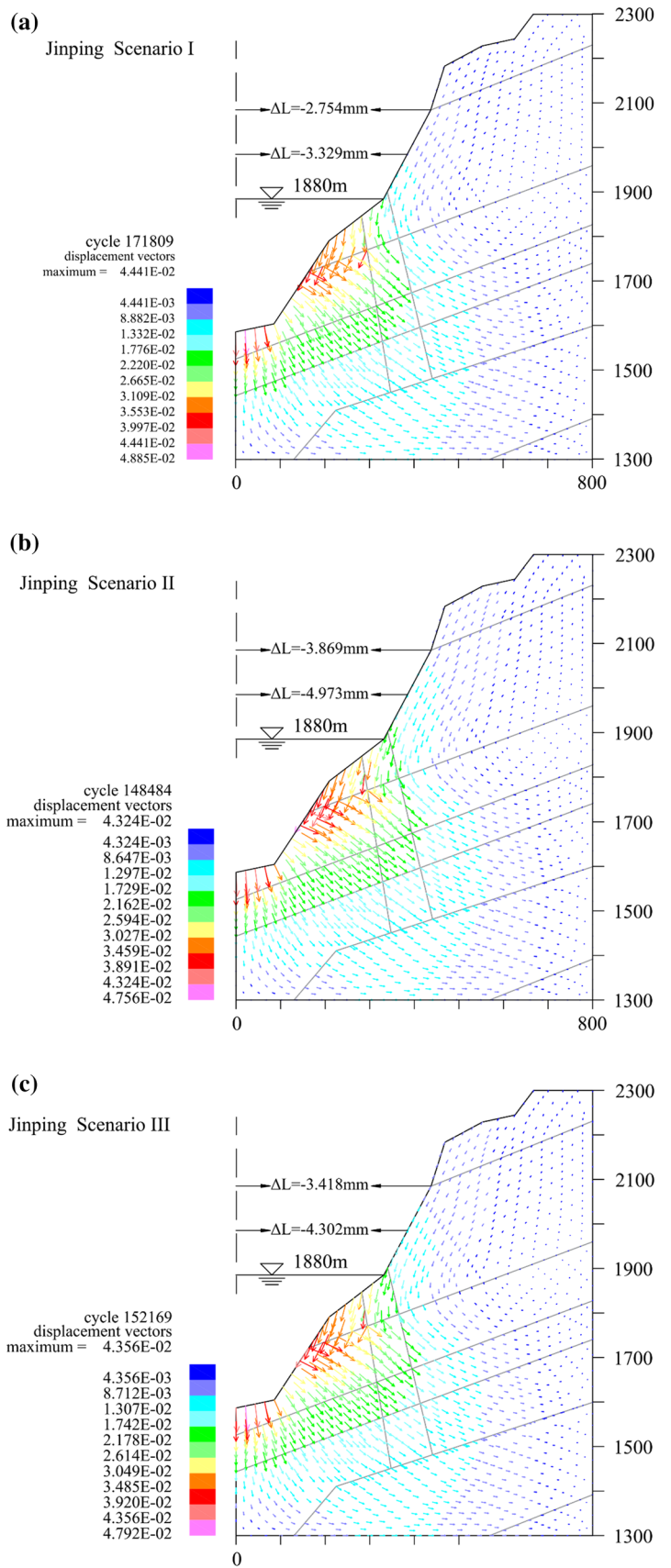
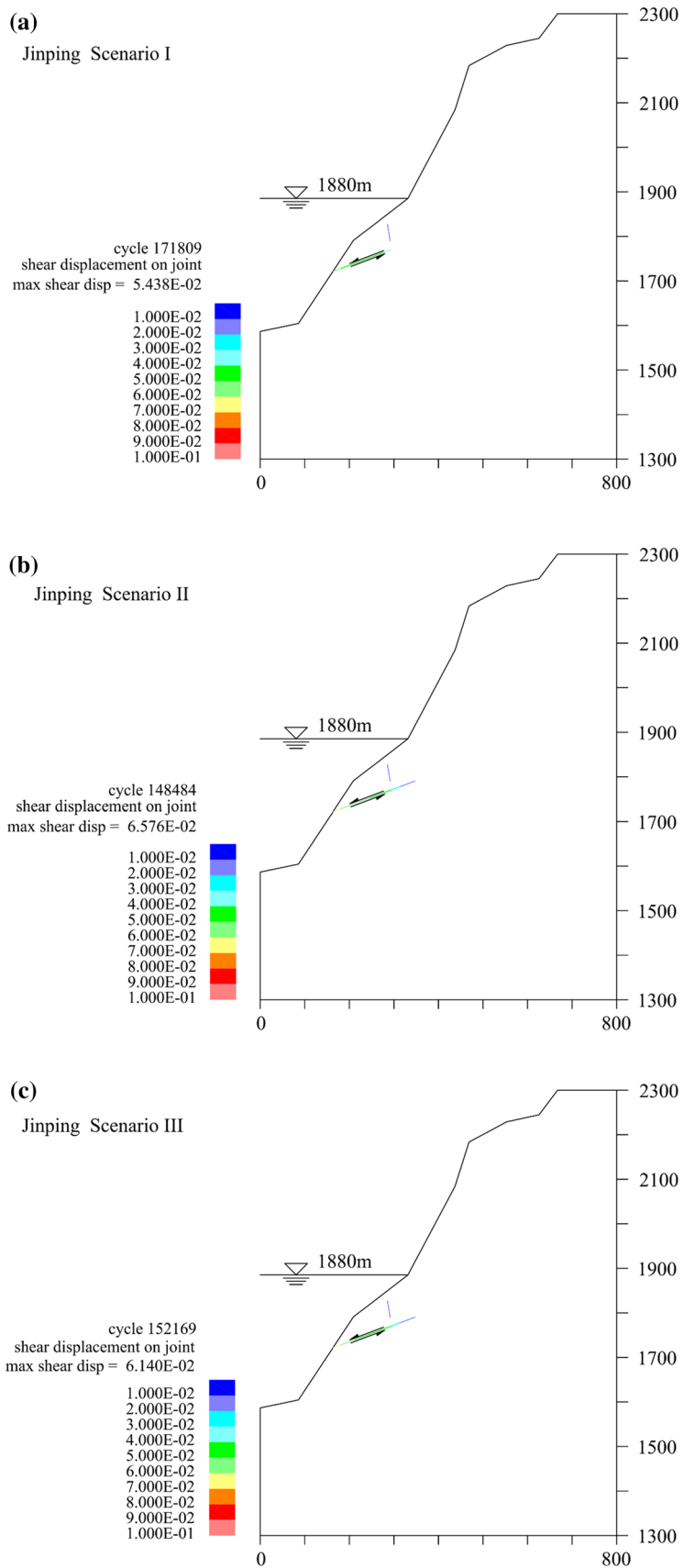


**Fig. 9** Fracture shear displacements in right bank slope of Jinping I high arch dam. **a** Scenario I. **b** Scenario II. **c** Scenario III



water–rock interaction plays an important role in the valley contraction.

## 5 Discussion and Conclusion

In reservoir bank slopes, multiple sets of joints, joint distribution and joint mechanical properties have a significant influence on slope deformation and stability. Those fractures that are subparallel to the slope surface are critical in determining slope deformation. Water–rock interactions can reduce fracture shear strengths and therefore worsen the stability of slopes. Two major mechanisms are responsible for the weakening of rock fractures. The first is a hydrogeological process during which water pressures in fracture voids alters the effective normal stress applied on fracture walls. The second is a physicochemical factor that reduces fracture cohesion and friction. Compared with mechanical and physical water–rock interactions, chemical water–rock interactions may need much longer time to reach a steady state. Binet et al. (2009) found that groundwater sulfate concentrations increased from 0.1 to 1 mmol L<sup>-1</sup> in the weeks following major landslide displacements and suggested that the unstable areas of slopes can be detected by associating major ions analyses. However, some experimental results showed that the weakening magnitude is not dependent on the duration of immersion (Zhao et al. 2017b). This indicates that chemical water–rock interactions are associated with mineral compositions of rocks.

Based on this numerical study, it can be concluded that slope displacements toward reservoirs may occur in fractured bank slopes, owing to water–rock interactions. This can qualitatively explain the observed valley contractions during the impoundment of high dams. Cheng et al. (2017) also studied valley contractions during the initial impoundment process using finite element modeling, and they attribute valley contractions to the shrinkage of the yield surface. The connected fractures would be full of water soon after the reservoir water level rises, whereas the development of micro-cracks/pores would take a much longer time. Therefore, fracture water pressure is responsible for the irreversible plastic deformation of rock masses (Cheng et al. 2017). The potential weakening of fractures due to physicochemical water–rock interactions may also need to be equivalently considered in continuum modeling of reservoir slope deformation.

In addition to the weakening of rock fractures induced by water–rock interactions, fracture initiation and growth may also occur during impoundment. The fracture voids may also be infilled by gouge materials, and the interaction between water and gouge materials should also be clarified in the future. Luo et al. (2016) showed that fracture surface roughness in nature may follow normal or lognormal

distributions, but a constant aperture was assumed in the present generic study. Examining whether the weakening of fractures induced by water–rock interactions is dependent on fracture surface roughness is also suggested for the future. Note that a few simplifications and assumptions were used in the case study, and thus, the results presented in this paper may or may not reflect the deformation behavior of real reservoir bank slopes. However, both mechanisms of water–rock interactions must be considered in assessing the stability of real reservoir bank slopes.

**Acknowledgements** The study was jointly supported by the National Natural Science Foundation of China (51509138, 51779123, 51739006), Beijing Natural Science Foundation (8152020), the Recruitment Program of Beijing Youth Experts (2014000020124G115) and the Open-end Research Fund of the State Key Laboratory of Water Resources and Hydropower Engineering Science (No. 2014SGG04).

## References

- Barla G, Antolini F, Barla M, Mensi E, Piovano G (2010) Monitoring of the Beaugard landslide (Aosta Valley, Italy) using advanced and conventional techniques. *Eng Geol* 116:218–235
- Barton N, Choubey V (1977) The shear strength of rock joints in theory and practice. *Rock Mech Rock Eng* 10:1–54
- Bidgoli MN, Jing L (2015) Water pressure effects on strength and deformability of fractured rocks under low confining pressures. *Rock Mech Rock Eng* 48:971–985
- Binet S, Spadini L, Bertrand C, Guglielmi Y, Mudry J, Scavia C (2009) Variability of the groundwater sulfate concentration in fractured rock slopes: a tool to identify active unstable areas. *Hydrol Earth Syst Sci* 13:2315–2327
- Chen Y, Cao P, Mao D, Pu C, Fan X (2014) Morphological analysis of sheared rock with water-rock interaction effect. *Int J Rock Mech Min Sci* 70:264–272
- Cheng L, Liu YR, Yang Q, Pan YW, Lv Z (2017) Mechanism and numerical simulation of reservoir slope deformation during impounding of high arch dams based on nonlinear FEM. *Comput Geotech* 81:143–154
- Cherblanc F, Berthouneau J, Bromblet P, Huon V (2016) Influence of water content on the mechanical behavior of limesonte: role of clay minerals content. *Rock Mech Rock Eng* 49:2033–2042
- Ciantia MO, Castellanza R, Crosta G, Hueckel T (2015a) Effects of mineral suspension and dissolution on strength and compressibility of soft carbonate rocks. *Eng Geol* 184:1–18
- Ciantia MO, Castellanza R, di Prisco C (2015b) Experimental study on the water-induced weakening of calcarenites. *Rock Mech Rock Eng* 48:441–461
- Geertsema AJ (2003) The shear strength of rock joints with special reference to dam foundations. Ph.D. Theses at University of Pretoria
- Itasca Consulting Group, Inc (2014) UDEC: Universal Distinct Element Code Version 6.0 User's Guide. Minneapolis, MN
- Jaeger JC, Cook NGW, Zimmerman RW (2007) Fundamentals of rock mechanics, 4th edn. Blackwell, Oxford
- Jing L, Stephansson O (2007) Fundamentals of discrete element methods for rock engineering: theory and application. Elsevier, Amsterdam, p 545
- Luo S, Zhao Z, Peng H, Pu H (2016) The role of fracture surface roughness in macroscopic fluid flow and heat transfer in fractured rocks. *Int J Rock Mech Min Sci* 87:29–38

- Maihemuti B, Wang E, Hudan T, Xu Q (2016) Numerical simulation analysis of reservoir bank fractured rock-slope deformation and failure processes. *Int J Geomech* 16:04015058
- Pellet FL, Keshavarz M, Boulon M (2013) Influence of humidity conditions on shear strength of clay rock discontinuities. *Eng Geol* 157:33–38
- Qi S, Wu F, Yan F, Lan H (2004) Mechanism of deep cracks in the left bank slope of Jinping first stage hydropower station. *Eng Geol* 73:129–144
- Qiao L, Wang Z, Huang A (2017) Alteration of mesoscopic properties and mechanical behavior of sandstone due to hydro-physical and hydro-chemical effects. *Rock Mech Rock Eng* 50:255–267
- Rode N, Homand-Etienne F, Hadadou R, Soukatchoff V (1991) Mechanical behaviour of joints of cliff and open pit. *Int J Rock Mech Min Sci Geomech Abstr* 28:277
- Song S, Feng X, Rao H, Zheng H (2013) Treatment design of geological defects in dam foundation of Jinping I hydropower station. *J Rock Mech Geotech Eng* 5:342–349
- Tuncay K, Corapcioglu MY (1995) Effective stress principle for saturated fractured porous media. *Water Resour Res* 31:3103–3106
- Van Eeckhout EM (1976) The mechanisms of strength reduction due to moisture in coal mine shales. *Int J Rock Mech Min Sci Geomech Abstr* 13:61–67
- Wasantha PLP, Ranjith PG (2014) Water-weakening behavior of Hawkesbury sandstone in brittle regime. *Eng Geol* 178:91–101
- Yang Q, Pan Y, Cheng L, Liu Y, Zhou Z, Xue L (2015) Mechanism of valley deformation of high arch dam and effective stress principle for unsaturated fractured rock mass. *Chin J Rock Mech Eng* 34:2258–2269
- Zhao Z, Yang J, Zhang D, Peng H (2017a) Effects of wetting and cyclic wetting-drying on tensile strength of sandstone with a low clay mineral content. *Rock Mech Rock Eng* 50:485–491
- Zhao Z, Yang J, Zhou D, Chen Y (2017b) Experimental investigation on the wetting-induced weakening of sandstone joints. *Eng Geol* 225:61–67
- Zimmerman RW, Bodvarsson GS (1996) Hydraulic conductivity of rock fractures. *Transp Porous Med* 23:1–30